Journal of Physics G: Nuclear and Particle Physics

PAPER

Improved background suppression for radiative capture reactions at LUNA with HPGe and BGO detectors

To cite this article: A Boeltzig *et al* 2018 *J. Phys. G: Nucl. Part. Phys.* **45** 025203

IOP Publishing Journal of Physics G: Nuclear and Particle Physics
J. Phys. G: Nucl. Part. Phys. **45** (2018) 025203 (18pp) https://doi.org/10.1088/1361-6471/aaa163

Improved background suppression for radiative capture reactions at LUNA with HPGe and BGO detectors

A Boeltzig[1,2,3], **A Best**[4,5], **G Imbriani**[4,5], **M Junker**[6], **M Aliotta**[7], **D Bemmerer**[8], **C Broggini**[9], **C G Bruno**[7], **R Buompane**[5,10], **A Caciolli**[9,11], **F Cavanna**[12], **T Chillery**[7], **G F Ciani**[1], **P Corvisiero**[12,13], **L Csedreki**[6], **T Davinson**[7], **R J deBoer**[2,3], **R Depalo**[9,11], **A Di Leva**[4,5], **Z Elekes**[14], **F Ferraro**[12,13], **E M Fiore**[15,16], **A Formicola**[6], **Z Fülöp**[14], **G Gervino**[17,18], **A Guglielmetti**[19,20], **C Gustavino**[21], **G Gyürky**[14], **I Kochanek**[6], **R Menegazzo**[9], **V Mossa**[15,16], **F R Pantaleo**[15,16], **V Paticchio**[16], **R Perrino**[16,25], **D Piatti**[9,11], **P Prati**[12,13], **L Schiavulli**[15,16], **K Stöckel**[8,22], **O Straniero**[23], **F Strieder**[24], **T Szücs**[14], **M P Takács**[8,22], **D Trezzi**[19,20], **M Wiescher**[2,3] and **S Zavatarelli**[13]

[1] Gran Sasso Science Institute (GSSI), Viale Francesco Crispi 7, I-67100 L'Aquila, Italy
[2] University of Notre Dame, Department of Physics, 225 Nieuwland Science Hall, Notre Dame, IN 46556, United States of America
[3] The Joint Institute for Nuclear Astrophysics (JINA)
[4] Università degli Studi di Napoli 'Federico II', Dipartimento di Fisica 'E. Pancini', Via Cintia, I-80126, Napoli, Italy
[5] Istituto Nazionale di Fisica Nucleare (INFN), Sezione di Napoli, Via Cintia, I-80126 Napoli, Italy
[6] INFN, Laboratori Nazionali del Gran Sasso (LNGS), Via Giovanni Acitelli 22, I-67100 Assergi, Italy
[7] SUPA, School of Physics and Astronomy, University of Edinburgh, Peter Guthrie Tait Road, Edinburgh EH9 3FD, United Kingdom
[8] Helmholtz-Zentrum Dresden-Rossendorf (HZDR), Bautzner Landstraße 400, D-01328 Dresden, Germany
[9] INFN, Sezione di Padova, via F. Marzolo 8, I-35131 Padova, Italy
[10] Università degli Studi della Campania 'L. Vanvitelli', Dipartimento di Matematica e Fisica, Viale Lincoln 5, Caserta, Italy
[11] Università degli Studi di Padova, Dipartimento di Fisica e Astronomia, via F. Marzolo 8, I-35131 Padova, Italy
[12] INFN, Sezione di Genova, Via Dodecaneso 33, I-16146 Genova, Italy
[13] Università degli Studi di Genova, Dipartimento di Fisica, Via Dodecaneso 33, I-16146 Genova, Italy
[14] Institute for Nuclear Research (MTA ATOMKI), PO Box 51, 4001 Debrecen, Hungary

0954-3899/18/025203+18$33.00

[15] Università degli Studi di Bari, Dipartimento Interateneo di Fisica, Via G. Amendola 173, I-70126 Bari, Italy
[16] INFN, Sezione di Bari, Via E. Orabona 4, I-70125 Bari, Italy
[17] Università degli Studi di Torino, Dipartimento di Fisica, Via P. Giuria 1, I-10125 Torino, Italy
[18] INFN, Sezione di Torino, Via P. Giuria 1, I-10125 Torino, Italy
[19] Università degli Studi di Milano, Dipartimento di Fisica, Via G. Celoria 16, I-20133 Milano, Italy
[20] INFN, Sezione di Milano, Via G. Celoria 16, I-20133 Milano, Italy
[21] INFN, Sezione di Roma, Piazzale A. Moro 2, I-00185 Roma, Italy
[22] Technische Universität Dresden, Institut für Kern- und Teilchenphysik, Zellescher Weg 19, D-01062 Dresden, Germany
[23] INAF Osservatorio Astronomico di Teramo, Via Mentore Maggini, I-64100 Teramo, Italy
[24] South Dakota School of Mines & Technology, Department of Physics, 501E St Joseph Street, Rapid City, SD 57701, United States of America

E-mail: axel.boeltzig@gssi.infn.it

Received 15 September 2017, revised 21 November 2017
Accepted for publication 13 December 2017
Published 18 January 2018

Abstract

Direct measurements of small nuclear reaction cross sections require a low background in the signal region of interest to achieve the necessary sensitivity. We describe two complementary detector setups that have been used for studies of (p, γ) reactions with solid targets at the Laboratory for Underground Nuclear Astrophysics (LUNA): a high-purity germanium detector and a bismuth germanate (BGO) detector. We present the effect of a customised lead shielding on the measured background spectra in the two detector setups at LUNA. We developed a model to describe the contributions of environmental and intrinsic backgrounds in the BGO detector measurements. Furthermore we present an upgrade of the data acquisition system for our BGO detector, which allows us to exploit the features of the segmented detector and overcome some of the limitations encountered in previous experiments. We conclude with a discussion on the improved sensitivity of the presented setups, and the benefits for ongoing and possible future measurements.

Keywords: gamma ray spectroscopy, nuclear astrophysics, background reduction, shielding, HPGe, BGO, summing detector

(Some figures may appear in colour only in the online journal)

1. Introduction

A vital input for stellar models in nuclear astrophysics is the cross section information for the nuclear reactions involved, as these cross sections determine the thermonuclear reaction rates

---

[25] Permanent address: INFN, Sezione di Lecce, Via Arnesano, I-73100 Lecce, Italy.

for a given stellar temperature. However, at energies that correspond to the temperatures of typical stellar scenarios, the charged particle cross sections can be so small that their direct measurement is challenging, as the reaction yield in an accelerator-based experiment is limited. One way to obtain cross section information in absence of a measurement is to extrapolate from data obtained at higher energies (see for example [1, 2]), but such extrapolations can introduce significant uncertainties in the cross section which in turn leads to large uncertainties of the reaction rates in stellar models. Direct measurements of the cross section at or as close as possible to the relevant energies can help to greatly reduce the reaction rate uncertainties and improve the precision of stellar models.

A high detection efficiency for the reaction products and a low background rate in the signal region of interest are crucial to achieve the required sensitivity for the direct measurement of a small cross section. The experiments to measure these small cross sections apply various techniques in order to successfully measure at low energies, close to the energy region of stellar scenarios. The approach to conduct such measurements deep underground has been pioneered by the Laboratory for Underground Nuclear Astrophysics (LUNA) [3, 4], located at the Gran Sasso National Laboratory (LNGS). The shielding provided by a massive overburden of rock drastically reduces the background induced by cosmic rays [5], including the flux of gamma rays and neutrons [6] created by muons. Likewise, detector setups for charged particles have been observed to benefit from lower background rates at an underground location [7]. Moreover, to reduce environmental background radiation, passive shielding around the detector becomes more effective than on the surface, where secondary radiation produced by cosmic ray interactions with the shielding itself acts as a further source of background [8]. With the reduced background at an underground location, the sensitivity of various experiments can be greatly enhanced in comparison to measurements on surface.

In this article we present the upgrades of two experimental setups in an underground environment: a high-purity germanium (HPGe) and a bismuth germanate (BGO) detector. These complementary detector systems have been used for past cross section measurements at LUNA, and have recently been upgraded with a lead shielding and an improved data acquisition (DAQ) system. These upgrades were installed in order to enhance the sensitivity of the setups for currently ongoing measurements [9], and for future measurements planned at LUNA and the new LUNA MV.

We introduce the general features of the two detector setups in section 2, and present lead shielding for the detector setups and the upgraded DAQ system for the BGO detector in section 3. In section 4 we discuss the improvements due to the upgrades in comparison with past configurations of the same detectors. The improved sensitivity has facilitated the development of a model for the background contributions in the BGO detector, as we also show in the same section. Lastly, in section 5 we discuss the potential of the presented setup for future experiments and possible further improvements.

2. Measurement of low energy radiative capture cross sections at LUNA

2.1. General considerations

Several gamma-ray detection techniques are employed in experimental nuclear physics, depending on the specific needs of each experiment and the nuclear properties under investigation. For cross section measurements of radiative capture reactions at LUNA, two different setups with complementary strengths are routinely used: a high-resolution but low-efficiency HPGe detector and a high-efficiency but low-resolution BGO calorimeter. The two setups offer distinct ways of distinguishing the signal of the studied reaction from background caused either by environmental and intrinsic backgrounds or by spurious reactions from interactions of the bombarding beam with impurities in the target material, as we will discuss below.

2.2. HPGe detector

HPGe detectors provide excellent energy resolution (e. g. 2.2 keV at a gamma-ray energy of 1.33 MeV, corresponding to a relative energy resolution of better than 0.2%). The full energy peak efficiency of an HPGe detector depends on the size of the germanium crystal and the distance of the source from the detector. It is often compared to a $3'' \times 3''$ NaI(Tl) scintillation detector at 1.33 MeV in a distance of 25 cm, which is then referred to as 100% relative efficiency. Achievable absolute full energy detection efficiencies are typically on the order of a few percent for 1 MeV gamma rays, owing to the limited volume of the crystal and the relatively low interaction probability of gamma rays in germanium. This efficiency decreases quickly for increasing gamma ray energies.

Multiple gamma rays can be emitted in a single radiative capture reaction. The likelihood of detecting more than one of these photons in an event, i.e. true coincidence summing, is a function of detection efficiency for the individual gamma rays. Although small in a typical HPGe detector setup, coincidence summing effects can be critical for the measurement of weak direct transitions or in geometries with relatively large detection efficiencies, i.e. small distances between detector and source. Summing effects have to be accounted for in the calibration of the HPGe detectors and the analysis of data acquired with them.

HPGe detectors allow for the identification of individual gamma-ray energies, which can then be attributed to the nuclear reactions under study or to background sources (see e g. [10]), even with limited prior knowledge of the possible contributions.

The setup we describe uses a coaxial HPGe detector (ORTEC GEM-120225-P-ST) that has a relative efficiency of 120%.

2.3. BGO detector

BGO ($Bi_4Ge_3O_{12}$, BGO) is a scintillating material with a very large gamma ray absorption efficiency ($Z_{\mathrm{Bi}} = 83$, density 7.13 g cm^{-3}) that can be manufactured in large sizes. A disadvantage of a BGO detector compared to an HPGe detector is the limited energy resolution of about 11% FWHM at 1.33 MeV.

The BGO detector we describe here has been employed in several past measurements of low yield radiative capture reactions at LUNA [11, 12]. The setup and application of the detector was first described in [13]. The detector is made of an array of six prismatic crystals, each 28 cm long and with a trapezoidal base area of 52 cm^2. The segments are arranged around a cylindric borehole, so that the target can be placed at the centre of the detector with a radial thickness of at least 7 cm of BGO around (see figure 1). With the target at the centre of the detector, a close to 4π solid angle coverage is achieved. Gamma rays produced in the target are absorbed very efficiently within the sensitive detector volume, and the efficiency decreases only slowly with gamma ray energy. Each of the six crystals is optically isolated and coupled to a $2''$ diameter photomultiplier tube (Hamamatsu R1847-07) at one end.

Each crystal covers only one sixth of the solid angle of the full detector around the target. Summing effects are expected, owing to the significant detection efficiency of a single crystal, but still limited. Considering all crystals as a whole, a sum energy spectrum is obtained, for which the large solid angle coverage enhances summing effects for gamma ray cascades. The summing effect is illustrated for the example of a simple two-step cascade in figure 2.

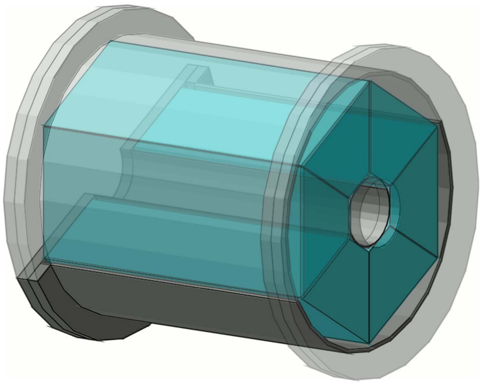

Figure 1. Sketch of the segmented BGO detector used at LUNA. Geometry as implemented in the Geant4 simulation; the PMTs are not shown.

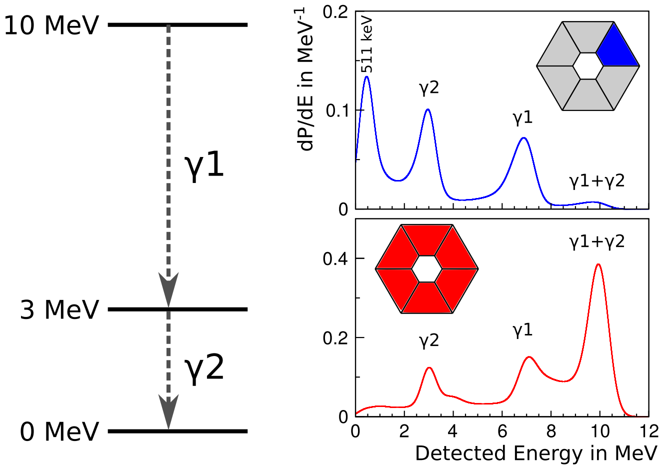

Figure 2. Illustration of single and sum spectra for a simple decay scheme with a cascade of two gamma rays (that are isotropically emitted and have no angular correlation) as obtained in a Geant4 simulation. The enhanced efficiency for detection of the full gamma energy in the full detector (bottom) is evident. Summing, on the other hand, is limited in the case of an individual crystal, and the peaks at the individual gamma ray energies are more prominent as the detection of both gamma rays in the same segment is less likely (top).

The region of interest in the sum energy spectrum is given by the peak corresponding to total absorption of all gamma rays. For a de-excitation of the daughter nucleus to the ground state in a radiative capture reaction, the total energy released as gamma rays is given by the Q-value plus the centre of mass energy of the entrance channel. The advantage of the summing detector for low-energy cross section measurements becomes clear for reactions with large Q values, where the region of interest is located at higher energies than most environmental and intrinsic backgrounds. Analysing the distribution of the energy deposition amongst the individual crystals may yield additional information related to the energy of single gamma rays in the cascades. Although the identification of unknown gamma rays can be difficult, owing to the limited energy resolution of the detector, this information from the individual segments can be valuable nonetheless. The number of detector segments that register an energy deposition, for example, is closely related to the gamma ray multiplicity of an event. If the gamma ray cascades associated with the observed reactions and backgrounds are known, the segmentation of the detector can therefore be exploited to identify and discriminate background events.

Past measurements at LUNA have used different DAQ setups for this detector. A measurement of ^{25}Mg(p, γ)^{26}Al [12] used the setup described in [13]: each PMT signal was capable of generating an acquisition trigger via a constant fraction discriminator, and a trigger in any of the six channels caused the conversion of the signals in all channels by an ADC (with a conversion time of 15 μs). The events were saved individually (list mode acquisition). From this event data, the energy spectra of each individual crystal could be obtained as well as a sum spectrum of the total energy registered in all crystals in a triggered event. For the measurements of the ^{14}N(p, γ)^{15}O cross section [11], the analogue sum of the six PMT signals was recorded with a multichannel analyser. This setup had the advantage of being fast, at the cost of missing information on the segmentation.

3. Custom shielding and BGO DAQ upgrade

3.1. Lead shielding

To further reduce environmental backgrounds in experiments at the solid target setup at LUNA, a new shielding has been designed for use with either the BGO or the HPGe detector on this beam line. The BGO detector can be placed at the centre of the shielding, the HPGe detector can either be mounted at 0° (to place the detector head-on), or at a 55° angle (to reduce the effect of unknown angular distributions as the Legendre polynomial P_2 vanishes at this angle) to the beam axis. The configurations for both detectors are shown in figure 3. The thickness of the lead shielding is 10 cm for the BGO detector and 15 cm for the HPGe detector (except for in- and outlet along the beam axis and an inlet in the 55° direction when the HPGe detector is in place). As the targets have to be replaced frequently in a typical solid target experiment, an important feature of this shielding setup is the easy access to the target, which is achieved by mounting the lead shielding on rails, so that the upstream and downstream parts can be easily separated. The additional lead piece at 55° is also mounted on rails and can be pulled away from the target, together with the mounted detector.

3.2. Digital BGO DAQ system

As described in section 2.3, the signal acquisition on a single-crystal level is advantageous. Critical aspects for a DAQ system that define the performance for a summing detector are the conversion time for a single event (which determines the acquisition dead time) and the coincidence event time window, i.e. the time period in which two events in different crystals have to be considered as associated with the same physical event.

We installed a new acquisition setup, with the aim to record event information for the creation of single and sum spectra, with a shorter event time window and reduced conversion times in comparison to the previously used setups. The individual PMT signals are preamplified (ORTEC Model 113) and acquired with a digitiser (CAEN V1724, 100 MS/s, 14 bit) that is equipped with pulse height analysis firmware (CAEN DPP-PHA), which implements a trapezoidal shaping algorithm [14]. An input rise time of 3.0 μs and a decay time of 30 μs were set as parameters for the shaping algorithm, corresponding to the properties of the preamplified input signals. Each channel is triggered independently and the

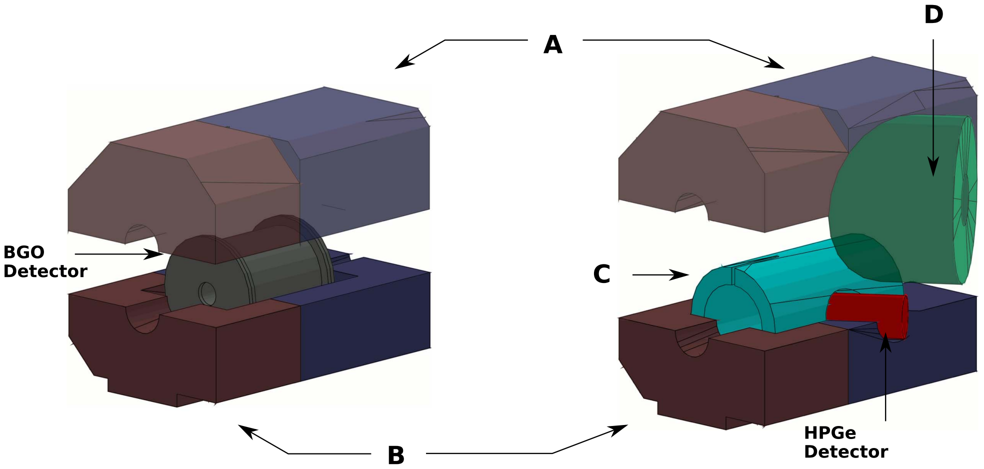

Figure 3. Sketches of the modular lead shielding for the BGO detector (left) and HPGe detector at 55° (right). The transparent top part is shown lifted to reveal the inside of the shielding. The beam line enters through the openings that are visible on the front left sides of the sketches. Beam line and target are omitted for clarity. Left: the BGO detector rests in the downstream part of the shielding, and can be retracted with this part of the shielding (A) to access the target, while the upstream part of the shielding (B) stays in place. Right: an additional cylindrical lead inset (C) and a block of lead (D) around the detector are used in this HPGe detector configuration (shown at 55°).

converted individual events with timestamps and energy information are written to disk. In the offline analysis, PMT signals occurring in a given coincidence time window are used to obtain a sum energy spectrum.

An advantage of the upgraded DAQ is the absence of digitisation dead time. The accidental pile-up of two events in one crystal can be identified if they are at least separated by the input rise time [15], which allows for lower accidental pile-up rates. The effect of the coincidence time-window is studied and optimised offline. On the one hand, this window needs to be large enough to include all registered events for a given physical signal, but on the other hand it should not be longer than necessary as this increases the probability for random summing (i.e. the accidental detection of gamma rays from two or more independent sources that occur in the time window of one event). Analysing the distribution of the time difference between consecutive events in any two detector segments (figure 4(a)), two contributions can be distinguished: true coincidences (dominant in the figure for the first 0.2 μs) and random coincidences. The former contribution occurs in a short time-window after the first event, whereas the latter component follows an exponential distribution with a significantly longer time constant. For the presented measurements with this setup, a coincidence time window of 3.5 μs was chosen (i.e. slightly larger than the input rise time).

The effect of the coincidence event time window on the level of pile-up can be illustrated by choosing different values for this window to create the sum spectrum. The results for an unshielded background run are shown in figure 4(b). The reduction of the coincidence event time reduces the background rate in the energy region between 3 and 6 MeV. As the probability for random summing scales with the event rate to the power of two, the effect would be less pronounced in a shielded background run.

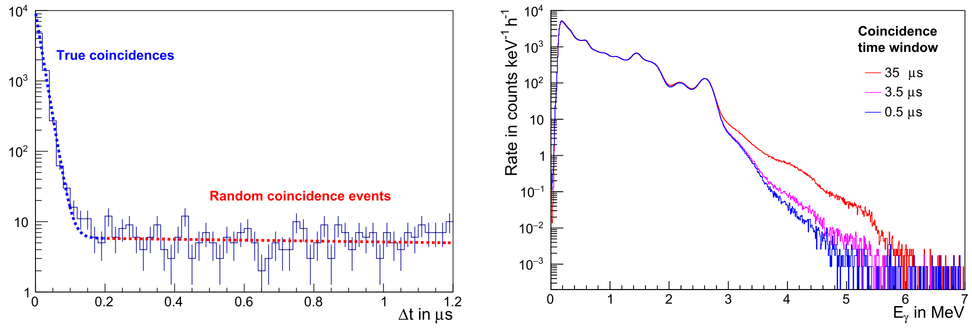

(a) Histogram of time difference between two consecutive events in two different crystals of the detector.

(b) Sum energy spectra for the same background measurement (unshielded BGO detector underground), obtained using different coincidence time windows.

Figure 4. Illustration of true coincidences and random pile-up in the distribution of time differences between consecutive events (a), and influence of the chosen coincidence time window on the obtained sum spectrum (b). In (a) true coincidence signals, caused by the same physical event, are clearly visible within the first 0.2 μs (---). At larger time differences (---) random coincidences of independent events dominate the distribution. In (b) the reduction of the contribution from accidental pile-up with decreased length of the coincidence event time window (— > — > —) is most pronounced in the energy region between 3 and 6 MeV.

4. Background measurements and modelling

The presented background measurements of the different setups were taken in the surface laboratories of LNGS (Assergi, Italy; approximately 1000 m above sea level) and in the LNGS underground laboratory at the location of the current LUNA accelerator (LUNA400).

4.1. HPGe detector

Different background measurements with the HPGe detector are shown in figure 5: a measurement on surface, the unshielded detector underground, and the detector in the new shielding.

Thanks to the energy resolution of the HPGe detector, distinct lines in the gamma ray spectra can be identified by their energy and linked to their sources. The majority of the background peaks can be attributed to primordial long-lived radioactive nuclides, or their decay chains [16], as indicated in figure 5. At energies above the highest gamma ray lines from natural radioactivity, a continuous background caused by cosmic radiation can be observed on surface, which underlines the motivation for a detector setup underground where the cosmic ray background is greatly reduced.

Count rates of prominent background lines are summarised in table 1. The strong suppression of background from cosmic rays is evident: the background at energies above 3.3 MeV (i.e. above the visible environmental gamma line with the highest energy) is reduced by three orders of magnitude underground compared to measurements on the surface. The strengths of environmental gamma ray backgrounds strongly depend on the surroundings of the detector, namely the content of radionuclides in the environment (e.g. uranium or thorium in the rock, or radon in the air), rather than the depth of the location. These background rates may also be subject to fluctuations in time [17], caused by changes in environmental

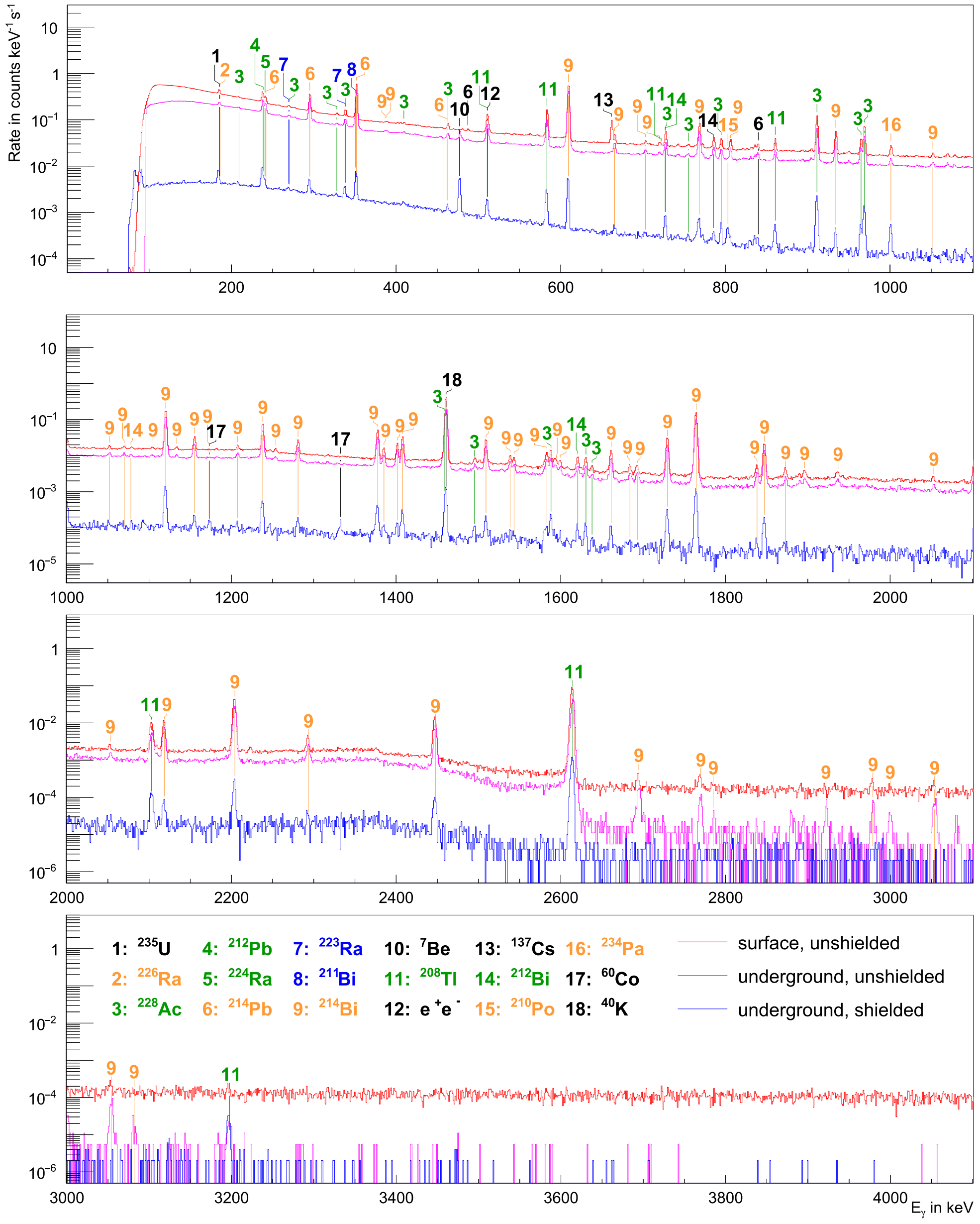

Figure 5. Background spectra acquired with the same HPGe detector: — unshielded on surface, — unshielded underground, and — fully shielded underground with the presented setup. The colours of the nuclides correspond to the decay chain they belong to: ^{238}U, ^{235}U, ^{232}Th, others.

conditions (such as the radon concentration in the air that depends on the ventilation of the location).

With this caveat in mind, a comparison of the background measurements underground with and without the lead shielding yields a substantial reduction of the environmental gamma

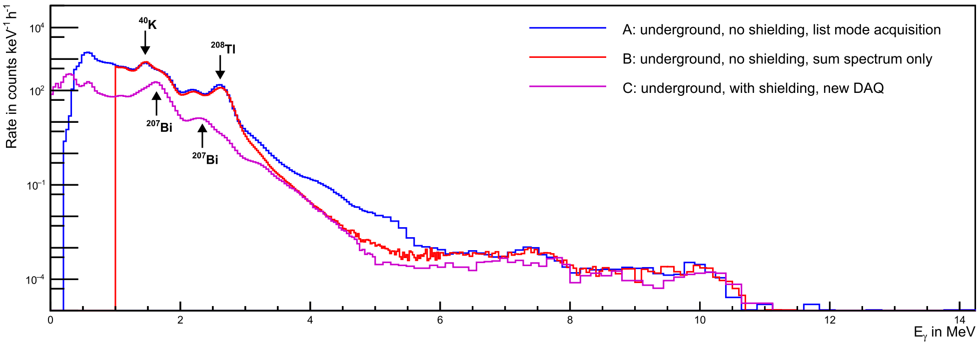

Figure 6. Background measurements (sum spectra) obtained with the BGO detector and the different DAQ setups described in section 2. The spectra for setup C was created using a coincidence time window of 3.5 μs.

Table 1. Comparison of count rates for different locations and shielding configurations of the same HPGe detector, corresponding to the spectra in figure 5. Entries denoted by 'n/a' are omitted, as the ambient radioactivity depends on the level of radioactivity in the environment of the detector, rather than the depth of the location. Rates are given in counts h^{-1} (peaks) and counts keV^{-1} h^{-1} (continuum).

			Surface	Underground	
Isotope	E_γ/keV	Origin	Unshielded	Unshielded	Shielded (this setup)
^{40}K	1461	Primordial	n/a	2190(10)	14.8(3)
^{214}Bi	1764	^{238}U chain	n/a	1260(15)	12.9(3)
^{208}Tl	2615	^{232}Th chain	n/a	680(15)	15.2(3)
Various	3300–6000	Cosmic	$3.30(2) \times 10^{-1}$	$2.4(4) \times 10^{-4}$	$1.9(2) \times 10^{-4}$

ray background: by factors of approximately 45, 100 and 150 for the ^{208}Tl, ^{214}Bi and ^{40}K lines, respectively. In massively shielded setups on surface, peaks associated with fast neutron scattering in the shielding material occur in the background spectrum [8]. No such peaks are visible in the shielded spectrum underground (as previously noted in [18]). A peak at 803.3 keV corresponds to the deexcitation of ^{206}Pb*, which can result from the decay of ^{210}Po or from fast neutron scattering on lead. As two other peaks of (n, n′) on lead (at 569.7 keV and 1063.3 keV from ^{207}Pb (n, n′)) that were observed in [8] are not visible in the background spectrum presented here, we conclude that the 803.3 keV line is at least predominantly caused by the decay of ^{210}Po. The ^{7}Be decay line that is observed in the spectra taken underground is attributed to activation of light elements, e.g. ^{6}Li or ^{10}B contaminants in the targets, by proton beam-induced reactions prior to the background measurements.

4.2. BGO detector

Background sum spectra of previous ^{25}Mg(p, γ)^{26}Al (setup A) and ^{14}N(p, γ)^{15}O (setup B) experiments, compared to the current upgraded setup (C) are shown in figure 6. The spectra of A and B are very similar up to 3 MeV and above 6 MeV. In the intermediate energy region, the background rates are significantly lower in setup B. This is consistent with the effect of a longer coincidence event time window in setup A, as demonstrated earlier (figure 4(b)). The background rates in setup C are consistently lower than for the other two setups, except for a small energy region around 4 MeV, where the rates of A and C are comparable. The background reduction of the shielded setup C compared to setups A and B is most pronounced at low gamma ray energies. The prominent background radiation peaks of ^{40}K and ^{208}Tl are efficiently suppressed by the shielding, and peaks from the underlying intrinsic background of ^{207}Bi, typical for BGO detectors [19], become visible.

4.3. BGO detector background model

To better understand the differences in the observed background spectra, it is important to identify and quantify the individual contributions to the background spectrum. Such a background model can then also serve as a tool to study the potential for further measures to reduce the background rates.

We recall that, as for the HPGe detector, the main sources of background follow from natural radioactivity or from cosmic radiation. In both cases the primary radiation can either directly deposit energy in the detector, or initiate reactions whose secondary particles can lead to a detectable energy deposition. An important example for secondary radiation are neutrons, e.g. from (α, n) reactions. Radioactivity can be attributed either to primordial radionuclides and their decay chains, or nuclides from activation of materials by cosmic rays.

Gamma rays from environmental radioactivity can be detected directly in the sensitive BGO volume. Intrinsic radioactivity in the BGO can deposit energy from α, β or γ radiation, depending on the decay. Due to quenching effects, the light output for α radiation is smaller than that for electrons (primary electrons from β decay or secondary electrons from the interaction of γ radiation).

For a quantitative understanding of the background contributions, we developed a model based on Geant4 (version 4.10.02 [20] with 'Shielding' physics list). Environmental backgrounds were modelled assuming that the primary particles for decays were homogeneously distributed in the considered volumes. For the radiative capture of thermal neutrons we used the cross sections from [21], and assumed that the capture events are distributed homogeneously within the detector (i.e. that the attenuation of the neutron flux is negligible). For the gamma rays following these captures we used a customised particle generator that incorporates the available gamma ray branching information for the daughter nuclides [22, and references therein].

Energy depositions in the crystals from (primary or secondary) charged particles were saved for each crystal individually. We applied quenching to the energy deposition of α particles (from intrinsic radioactivity), characterised by a quenching constant k_B following [23]. Finally we convoluted the resulting spectra with a Gaussian energy resolution function with a variance that is a linear function of the energy, assuming a quadratic relation between the (quenched) energy deposited in the crystal and the visible signal in the detector. This procedure yields response spectra for each radioactive nuclide in the respective volumes and the capture events from thermal neutrons. Introducing a pile-up time window τ as an additional parameter, we also calculated the spectra for random summing for the combination of any two components, as well as pile-up of consecutive radioactive decays (i.e. Bismuth–Polonium coincidences).

In a maximum-likelihood fit to the background data with setup C (simultaneously fitting single crystal and sum spectra), we determined the weight of each contribution and the parameters for the response of each crystal (energy calibration and resolution). We assumed that the short-lived sections of the decay chains in each material are in equilibrium, but the equilibrium of the overall chain can be broken at elements with larger half lives. The results of this fit are shown in figure 7 for the sum spectrum, and figure 8 for a selected single spectra.

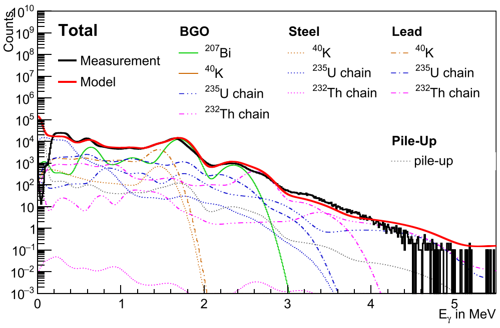

Figure 7. Comparison between measured background sum spectrum (—) and calculated one (—) for the BGO detector in the new shielding and with the new DAQ. Individual contributions from various radioactivity sources in different parts of the setup are shown by colour lines. Not shown here is the fit result for the thermal neutron capture background, owing to the limited statistics in this dataset.

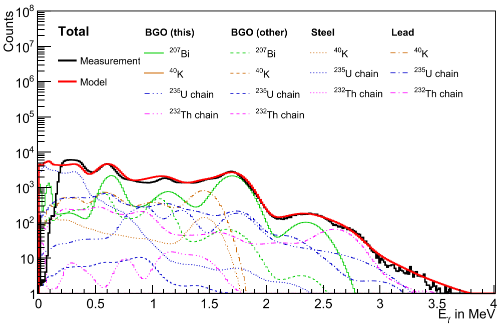

Figure 8. Background spectrum (—) for a single crystal of the BGO detector (new shielding and new DAQ) and associated fit (—). Contributions from different volumes of the detector and its environment are also shown (colour lines).

The background spectrum of one crystal is visibly different from the other five crystals in the region around 1.5 MeV, with what appears to be a lower content in ^{207}Bi and an undetermined additional intrinsic background contribution at a (quenched) energy deposition of 1.5 MeV (see figure 9). The detector response in this region (tested with the 1.33 MeV gamma line ^{60}Co) was similar among all crystals. The modelled intrinsic activities of ^{207}Bi are about half as large for this one crystal, compared to the other five crystals. It has to be noted, that the sensitivity to the location of some of the external backgrounds in this model is limited. For example, the shape of the signal of ^{40}K in the steel casing of the detector or in the lead around it is very similar, so that the model parameters for the activities in the two volumes are strongly anti-correlated and individually have a large uncertainty.

The background in the region between 6 and 12 MeV is dominated by thermal neutron capture on various isotopes of Ge, Fe, Cr and Ni (figure 10). For this fit, the capture cross sections for each element were allowed to vary slightly (to account for uncertainties in the description of the involved materials). In the best fit case, the scale factors to Ge, Cr and Ni were close to unity; enhancing the contribution of the neutron capture on iron by 20% significantly improved the fit. This may be an indication of an unaccounted contribution of iron, e.g. in other objects surrounding the detector in this unshielded measurement. A long

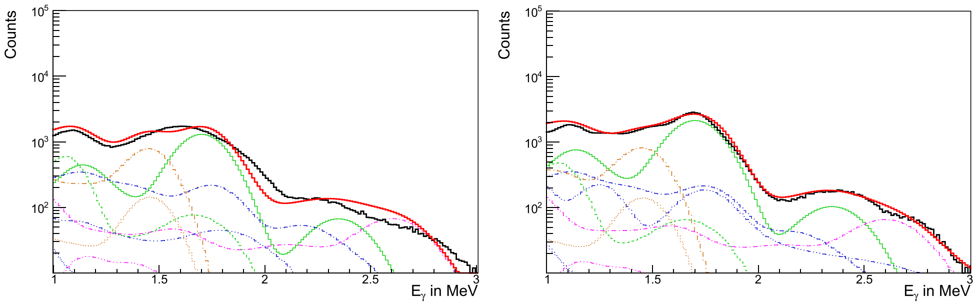

Figure 9. Zoomed single spectra models for one typical crystal (left) and a crystal with an atypical broader feature of unknown origin at 1.5 MeV (right). The feature is too broad and too low in energy to be fitted with ^{207}Bi (—). The energy resolution of the crystals was comparable (see text for details). Legend of components as in figure 8.

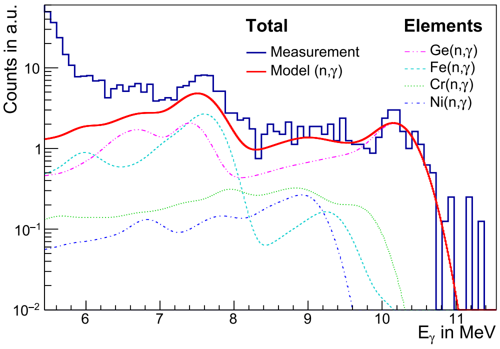

Figure 10. Contributions of radiative thermal neutron capture to the sum spectrum of an unshielded detector, by element on which the capture occurs. The dominating contributions come from germanium (BGO crystals) and iron (steel casing). The steeply falling background to the left is caused by intrinsic backgrounds and environmental gamma rays (not modelled here).

background measurement in a configuration for which the materials surrounding the detector are well known would be required to investigate this further.

Using the thermal neutron capture cross sections, the neutron flux can be estimated from the fit of the capture gamma ray spectrum. Considering the capture component on germanium, which dominates at higher energies, one obtains a flux of $7.0 \times 10^{-7}\,\mathrm{cm}^{-2}\,\mathrm{s}^{-1}$, with a statistical uncertainty of 6%. Between 8.5 and 11 MeV, the discrepancy between fitted and measured spectrum is on the order of 20%. The capture cross section on ^{73}Ge that dominates in this energy region ($Q = 10.2$ MeV) has a relative uncertainty of only 3% [21]. Considering the difference between fitted and measured spectrum, we conservatively estimated the systematic uncertainty of the flux to be 25%, to account also for unknown branching ratios in the simulation of the spectral shapes. In the simulation, levels with unknown branching ratios were assumed to directly decay to the ground state. As events with lower gamma-ray multiplicities have a larger probability to deposit their full energy in the detector, this assumption may systematically distort the spectrum towards events with larger energy depositions. This is a possible reason for the discrepancy between the model and the measurement, as the model predicts fewer events at lower deposited energies of the neutron capture region of the spectrum.

This uncertainty yields a result for the flux of $(7.0 \pm 0.4^{\text{stat.}} \pm 1.8^{\text{syst.}}) \times 10^{-7}\,\text{cm}^{-2}\,\text{s}^{-1}$.

The neutron flux obtained with this method is higher than the result of measurements with ^{3}He counters at LUNA, close to the BGO detector location: $(3.2 \pm 0.9^{\text{stat.}} \pm 0.4^{\text{syst.}}) \times 10^{-7}\,\text{cm}^{-2}\,\text{s}^{-1}$, but compatible within the set of neutron flux measurements at LNGS [6, and references therein]. A possible temporal variation of the neutron flux may need to be taken into account for the comparison. Another contribution to the BGO neutron capture background may come from non-thermal neutrons that are captured with a lower cross section, or become thermalised in the detector material and thus increase the number of capture events (in comparison to the light ^{3}He counters).

A reduction of the rate in the region of neutron-induced backgrounds by about a factor of 2 is observed with the shielded setup, compared to the unshielded setups. This reduction is compatible with the attenuation of thermal neutrons by the lead shielding as determined in the Geant4 simulation.

5. Conclusions and outlook

5.1. Results

The effective reduction of environmental backgrounds by the lead shielding has been demonstrated for both detector types by comparing shielded background measurements with data from previous experiments.

The environmental background count rates in the HPGe spectrum are reduced over the full energy range. Compared to other, more complex shielding setups (such as [18] on LUNA’s gas target line, or [24]) the environmental background levels with this setup are higher. The rates are nonetheless significantly lower than in previous setups used at LUNA’s solid target station that provided the necessary frequent access to the target. Following the principles of the cited setups, the background reduction caused by the shielding presented here could be further improved by flushing the surroundings of the detector with clean nitrogen to reduce airborne backgrounds from radon, or by replacing the inner part of the shielding with selected material of low intrinsic radioactivity.

In the BGO detector spectrum, the lead shielding improved the background count rate in every part of the spectrum up to 11 MeV, except for a small region at 4 MeV, where the background rates have been shown to be dominated by intrinsic backgrounds, and comparable background rates are observed with and without shielding. In the configuration with the lead shielding, the background spectrum of the BGO detector at low energies is strongly characterised by intrinsic backgrounds. In particular, the intrinsic background of ^{207}Bi is an irreducible contribution for detected energies up to approximately 2.5 MeV. Depending on the requirements of future experiments with this detector setup, measures can be taken to further reduce at least those non-beam-induced backgrounds that are not intrinsic to the BGO crystals. An example would be the application of more radiopure materials surrounding the detector. The precise origin of the backgrounds (e.g. steel casing or lead shielding) would have to be studied in dedicated measurements, as the BGO energy spectra in the presented configuration have a low sensitivity to the location/distance of the source for at least some of the nuclides. In view of the neutron capture background, material surrounding the detector should also not contain nuclides with large cross sections and Q values for radiative thermal neutron capture.

Neutron capture as the dominant background contribution at energies above the intrinsic background motivates the installation of an additional layer of shielding to absorb thermal neutrons. Such a shielding would be expected to reduce the neutron capture rate in all parts of the detector and therefore the background rate in the energy range 6–11 MeV. Preliminary tests, covering large parts of the lead shielding with additional 5 cm of borated polyethylene (5% boron content by mass), showed a promising further reduction of the background in this energy region of about a factor of 3. The permanent installation of a neutron shield, e.g. sheets of borated polyethylene, on this setup is under investigation.

5.2. Application in future experiments

With the improvement of the background rates of the presented setups, cross section measurements at lower energies, or the establishment of more stringent upper limits on the strengths of unobserved nuclear resonances are expected to become feasible. The reduced environmental gamma ray background was already beneficial for the HPGe experiments to measure ^{18}O(p, γ)^{19}F and ^{23}Na(p, γ)^{24}Mg, which will be the subject of forthcoming publications. As an outlook, we will briefly outline few examples of possible reactions whose potential to be measured at LUNA is affected by the achieved background reduction.

As an example for the HPGe detector setup, the reaction ^{12} C + ^{12}C can be considered a promising candidate for a measurement at the upcoming LUNA MV accelerator. A previous measurement [25] with a lead-shielded HPGe detector on surface studied the reactions ^{12}C(^{12}C, p)^{23}Na and ^{12} C(^{12}C, α)^{20}Ne by observing the transition from the first excited to ground state of the daughter nuclei ($E_\gamma = 440$ and 1634 keV respectively). As described in this reference, the experimentally accessible energy range can be greatly increased for an experiment in an underground location. As the regions of interest for these two transitions are dominated by environmental backgrounds, massive shieldings can reduce these background rates. A direct comparison of the backups in the surface experiment to the presented new setup is difficult, as no direct information on the background rates is provided in [25]. However, [25] notes that the background levels near the 1634 keV line is 50 times lower in the Slanic Prahova mine than in the surface experiment. Compared to the background data for a germanium detector with a relative efficiency of 22.8% and a 5 cm lead shielding in [26], the count rate of the 2615 keV line of ^{208}Tl is lower by approximately another factor of 7 and the rate of the 1461 keV line of ^{40}K lower by a factor of 38 in the setup presented here. The difference in relative efficiency between the two setups should additionally be taken into account to compare their sensitivity.

The presented setup offers the possibility for a solid target experiment with a significantly lower background rate than previously available on surface. Additional improvements of the shielding as discussed above are expected to further strengthen this advantage.

For the BGO detector we will investigate two examples that benefit from the background reduction in the high-energy part of the spectrum.

To demonstrate the effect of the reduced background on a cross section measurement with a significant influence of environmental backgrounds, we consider a measurement of the ^{14} N(p, γ)^{15}O cross section obtained with the BGO detector on the gas target setup at LUNA [11]. Figure 11(a) shows the spectrum as measured with the unshielded detector, whereas figure 11(b) shows the same data (lab background subtracted from measurement in 11(a)), on top of a randomly sampled background for a background rate that corresponds to the shielding test with 10 cm of lead and partial shielding of borated polyethylene. With the lower background rate, the same statistical uncertainty would be achieved with less accumulated charge on target (i.e. in a shorter run time, in this example by a factor of 2–3 with the lowest

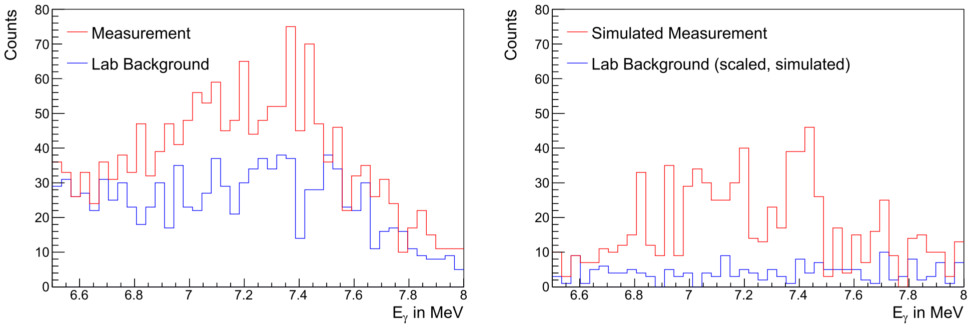

(a) Measured data as shown in [11, figure 10]. ($E_{\mathrm{beam}} = 80.9\,\mathrm{keV}, E_{\mathrm{eff}} = 70\,\mathrm{keV}$, 928 C accumulated charge).

(b) Computed spectrum with background scaled according to the results of tests with lead and borated polyethylene shielding.

Figure 11. Illustration of the hypothetical influence of the improved shielding on the sum spectrum in the region of interest for a measurement of ^{14}N(p, γ)^{15}O. In (a) the measurement (with an unshielded detector) is shown as in [11]. The plot in (b) shows the same signal over a randomly sampled (flat) background with a reduced rate.

measured background rate and assuming beam-induced backgrounds are negligible), or with the same accumulated charge the cross section could be measured at even lower energies. Although the measurement in [11] was conducted with an extended gas target and the presented shielding was designed for a solid target experiment, this example still holds. Solid targets have been used in other experiments to study reactions on nitrogen, and the general implications from studying this shielding would apply equally to a gas target.

As an example for a solid target experiment, we evaluate the reaction ^{17}O(p, γ)^{18}F, using nuclear properties as compiled in [27]: a narrow resonance of this reaction at a (centre of mass) energy of 66.0(3) keV dominates the reaction rate in the temperature range $T = 0.1$–0.2 GK. The strength of this resonance has not been measured directly yet, and is given as $\omega\gamma = 5.9^{+1.9}_{-1.1} \times 10^{-11}\,\mathrm{eV}$ in [27]. This resonance has recently been measured in the alpha channel [28], yielding an increased proton width (and with that a larger (p, γ) resonance strength) with respect to the literature value. In order to produce a conservative estimate we based our simulation on the central value of the older reference. We can calculate the expected reaction yield for Ta$_2$O$_5$ targets [10], assuming an enrichment of 90% in ^{17}O (as commercially available). The branching ratios for the resonance level in ^{18}F are known, so that the detector response can directly be obtained with the Geant4 simulation of the detector. To study the feasibility of such a measurement, we consider the example of an experiment of 6 weeks—3 weeks with an average current of 100 μA on target and 3 weeks of background measurement with beam off. The expected results for such a measurement for the different shielding configurations—randomly sampled from the simulated signal and a flat background—are shown in figure 12. Whilst the expected signal is hardly distinguishable in the unshielded case, with the lead shielding, and even more so in combination with the borated polyethylene shielding, a direct measurement of this resonance strength seems well within reach in terms of non beam-induced backgrounds. The potential for further background discrimination based on event topology (i.e. with the knowledge of the gamma ray cascades from the resonant reaction) has not been explored yet.

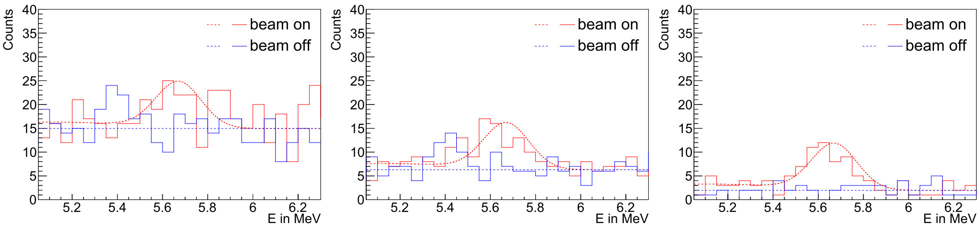

(a) Unshielded. (b) Lead shielding. (c) Lead shielding and borated polyethylene (tests).

Figure 12. Simulated distributions (--- / ---) and sampled outcome of a possible experiment (— / —) measuring on top of the 66 keV resonance of ^{17}O(p, γ)^{18}F with a solid Ta$_2$O$_5$ target (90% enriched in ^{17}O) for 21 days of beam on target and 21 days beam off, assuming a flat background with background rates obtained in measurements with different shielding configurations.

5.3. Summary

The solid target setup at LUNA has been upgraded with a customised lead shielding that can accommodate a BGO or HPGe detector. The BGO detector setup at LUNA has been upgraded with a new DAQ for a faster acquisition of the segmented detector signal. The new system is able to acquire at higher event rates and is less susceptible to accidental summing (pile-up) than previous setups.

A detailed model of the backgrounds in the shielded BGO detector suggested the possibility of further improvements of the environmental backgrounds in this detector with a neutron shielding. Preliminary results from tests adding borated polyethylene to the lead shielding are encouraging. The upgraded setup presented here will help to further increase the sensitivity to study weak radiative capture reactions at LUNA.

Acknowledgments

Design and installation support for the lead shielding by L Roscilli and the mechanical workshop of the University of Naples are gratefully acknowledged. The support of the mechanical workshop of the Gran Sasso National laboratory to install the shielding setup was greatly appreciated. The authors thank M Laubenstein for practical advice and discussions on the HPGe setup and backgrounds. The Monte Carlo simulations were performed on computing resources provided by the Gran Sasso Science Institute.

Financial support by INFN, the Deutsche Forschungsgemeinschaft (BE 4100/4-1) and OTKA (grant K120666) are also gratefully acknowledged. A Best acknowledges support through the STAR 2016 program of the University of Naples 'Federico II'.

ORCID iDs

A Boeltzig https://orcid.org/0000-0002-7209-2499
A Best https://orcid.org/0000-0001-8869-9757
I Kochanek https://orcid.org/0000-0001-8407-3589
R Perrino https://orcid.org/0000-0002-5764-7337

References

[1] Azuma R E *et al* 2010 *Phys. Rev.* C **81**
[2] Imbriani G *et al* 2012 *Phys. Rev.* C **85** 065810
[3] Costantini H, Formicola A, Imbriani G, Junker M, Rolfs C and Strieder F 2009 *Rep. Prog. Phys.* **72** 086301
[4] Broggini C, Bemmerer D, Guglielmetti A and Menegazzo R 2010 *Annu. Rev. Nucl. Part. Sci.* **60** 53–73
[5] Bellini G *et al* 2012 *J. Cosmol. Astropart. Phys.* JCAP12(2012)015
[6] Best A, Görres J, Junker M, Kratz K L, Laubenstein M, Long A, Nisi S, Smith K and Wiescher M 2016 *Nucl. Instrum. Methods Phys. Res.* A **812** 1–6
[7] Bruno C G *et al* 2015 *Eur. Phys. J.* A **51** 94
[8] Núñez Lagos R and Virto A 1996 *Appl. Radiat. Isot.* **47** 1011–21
[9] Boeltzig A, Pantaleo F R, Best A, Imbriani G, Junker M and Perrino R 2017 Status of direct ^{23}Na(p, γ)^{24}Mg and ^{18}O(p, γ)^{19}F cross section measurements underground at LUNA *JPS Conf. Proc.* **14** 020409
[10] Di Leva A *et al* (LUNA Collaboration) 2014 *Phys. Rev.* C **89** 015803
[11] Bemmerer D *et al* 2006 *Nucl. Phys.* A **779** 297–317
[12] Strieder F *et al* 2012 *Phys. Lett.* B **707** 60–5
[13] Casella C *et al* 2002 *Nucl. Instrum. Methods Phys. Res.* A **489** 160–9
[14] Jordanov V T and Knoll G F 1994 *Nucl. Instrum. Methods Phys. Res.* A **345** 337–45
[15] CAEN 2011 Digital Pulse Height Analyser, a digital approach to radiation spectroscopy (AN2508) (application note) (http://www.caen.it/csite)
[16] Heusser G 1995 *Annu. Rev. Nucl. Part. Sci.* **45** 543–90
[17] Bossew P 2005 *Appl. Radiat. Isot.* **62** 635–44
[18] Caciolli A *et al* 2009 *Eur. Phys. J.* A **39** 179–86
[19] Grigoriev D, Kuznetcov G, Novoselov I, Schotanus P, Shavinski B, Shepelev S, Shlegel V and Vasiliev Y 2009 Incidental radioactive background in BGO crystals *Proc. 1st Int. Workshop 'Radiopure Scintillators for EURECA' (RPScint'2008)* (arXiv: 0903.1539[nucl-ex])
[20] Agostinelli S *et al* 2003 *Nucl. Instrum. Methods Phys. Res.* A **506** 250–303
[21] Mughabghab S F 2006 Atlas of neutron cross section: thermal cross sections & resonance integrals (http://nndc.bnl.gov/atlas/atlasvalues.html)
[22] National Nuclear Data Center 2017 Information extracted from the NuDat 2 database (http://nndc.bnl.gov/nudat2/)
[23] Glasow R, Kampert K H, Löhner H, Beckmann P and Santo R 1985 *Nucl. Instrum. Methods Phys. Res.* A **228** 354–8
[24] Arpesella C 1996 *Appl. Radiat. Isot.* **47** 991–6
[25] Spillane T *et al* 2007 *Phys. Rev. Lett.* **98** 122501
[26] Margineanu R, Simion C, Bercea S, Duliu O, Gheorghiu D, Stochioiu A and Matei M 2008 *Appl. Radiat. Isot.* **66** 1501–6
[27] Angulo C *et al* 1999 *Nucl. Phys.* A **656** 3–183
[28] Bruno C *et al* (LUNA Collaboration) 2016 *Phys. Rev. Lett.* **117** 142502